Effective Spin-Mixing Conductance of Heavy-Metal–Ferromagnet Interfaces

Lijun Zhu,[1,*] Daniel C. Ralph,[1,2] and Robert A. Buhrman[1]
[1]Cornell University, Ithaca, New York 14850, USA
[2]Kavli Institute at Cornell, Ithaca, New York 14853, USA

(Received 1 March 2019; published 1 August 2019)

The effective spin-mixing conductance ($G_{\text{eff}}^{\uparrow\downarrow}$) of a heavy-metal–ferromagnet (HM-FM) interface characterizes the efficiency of the interfacial spin transport. Accurately determining $G_{\text{eff}}^{\uparrow\downarrow}$ is critical to the quantitative understanding of measurements of direct and inverse spin Hall effects. $G_{\text{eff}}^{\uparrow\downarrow}$ is typically ascertained from the inverse dependence of magnetic damping on the FM thickness under the assumption that spin pumping is the dominant mechanism affecting this dependence. We report that this assumption fails badly in many in-plane magnetized prototypical HM-FM systems in the nanometer-scale thickness regime. Instead, the majority of the damping is from two-magnon scattering at the FM interface, while spin-memory-loss scattering at the interface can also be significant. If these two effects are neglected, the results will be an unphysical "giant" *apparent* $G_{\text{eff}}^{\uparrow\downarrow}$ and hence considerable underestimation of both the spin Hall ratio and the spin Hall conductivity in inverse or direct spin Hall experiments.

DOI: 10.1103/PhysRevLett.123.057203

Interfacial spin transport is at the root of many spintronic phenomena, e.g., spin-orbit torques (SOTs) [1,2], spin magnetoresistance (SMR) [3,4], the spin Seebeck effect (SSE) [5–7], and spin pumping [8–16] in heavy-metal–ferromagnet (HM-FM) systems. The key factor determining the spin transmission and spin backflow (SBF) of a HM-FM interface [17,18] is the effective spin-mixing conductance [19]

$$G_{\text{eff}}^{\uparrow\downarrow} = G_{\text{HM-FM}}^{\uparrow\downarrow}/(1 + 2G_{\text{HM-FM}}^{\uparrow\downarrow}/G_{\text{HM}}), \tag{1}$$

where $G_{\text{HM-FM}}^{\uparrow\downarrow}$ is the bare interfacial spin-mixing conductance, $G_{\text{HM}} = 1/\lambda_s\rho_{xx}$, ρ_{xx}, and λ_s are the spin conductance, the resistivity, and the spin diffusion length of the HM layer, respectively. In inverse spin Hall effect (ISHE) experiments where spin currents are generated by spin pumping or the SEE, the measured voltage signals are proportional to $G_{\text{eff}}^{\uparrow\downarrow}\theta_{\text{SH}}$ [6–16]. Here θ_{SH} is the spin Hall ratio of the HM. For SOT experiments [20–23], the drift-diffusion analysis [4,17] predicts an interfacial spin transparency [19]

$$T_{\text{int}} = 2G_{\text{eff}}^{\uparrow\downarrow}/G_{\text{HM}} \leq 1 \tag{2}$$

when the HM thickness $d \gg \lambda_s$ and the interfacial spin-orbit coupling (ISOC) is negligible. Therefore, the measured dampinglike SOT efficiency per unit applied electric field is $\xi_{\text{DL}}^{E} \approx 2\, G_{\text{eff}}^{\uparrow\downarrow}\theta_{\text{SH}}/\rho_{xx}G_{\text{HM}}$. For SMR experiments, the measured resistance signals are proportional to $G_{\text{eff}}^{\uparrow\downarrow}\theta_{\text{SH}}^2$ [3,4]. As a consequence, for all of these techniques, any errors in the determination of $G_{\text{eff}}^{\uparrow\downarrow}$ will directly result in an incorrect evaluation of θ_{SH} and the spin Hall conductivity [$\sigma_{\text{SH}} \equiv (\hbar/2e)\theta_{\text{SH}}/\rho_{xx}$] of the HM; in general if $G_{\text{eff}}^{\uparrow\downarrow}$ is overestimated, θ_{SH} and σ_{SH} will be underestimated.

In practice, $G_{\text{eff}}^{\uparrow\downarrow}$, or equivalently $g_{\text{eff}}^{\uparrow\downarrow} = G_{\text{eff}}^{\uparrow\downarrow}h/e^2$, for a HM-FM system is typically determined by measuring the FM thickness (t_{FM}) dependence of the damping (α) of in-plane magnetized bilayers based on the standard model, where the t_{FM} dependence is attributed only to the enhancement of α by spin pumping into the HM layer [7–12,24–28], i.e.,

$$\alpha = \alpha_{\text{int}} + G_{\text{eff},\alpha}^{\uparrow\downarrow}\frac{g\mu_B h}{4\pi M_s e^2}\, t_{\text{FM}}^{-1}, \tag{3}$$

where α_{int} is the thickness-independent "intrinsic" damping of the FM layers, M_s the saturation magnetization of the FM layers, g the g factor, μ_B the Bohr magnetron, and h Planck's constant, respectively. The apparent values of $G_{\text{eff},\alpha}^{\uparrow\downarrow}$ obtained by this method have been widely used to estimate θ_{SH} and σ_{SH} in many spin-pumping–ISHE, SEE-ISHE, SMR, and SOT experiments [4,6,8–11,13–16,24].

In this Letter, we report that spin pumping is a relatively minor contribution to α for the most commonly studied in-plane magnetized HM-FM systems in the nanometer thickness and gigahertz frequency regions that are of most interest for spintronics. In contrast, two-magnon scattering (TMS) [29,30] predominantly determines the t_{FM} dependence of α. When ISOC is sufficiently strong, the second largest contribution can be spin memory loss (SML) [12,31–35]. Neglecting TMS and SML, particularly the former, when analyzing measurements of α in HM-FM

TABLE I. Details of the Pt-FM sample series. T_a is the annealing temperature. The estimates for α_{int} labeled "no TMS" are obtained from the intercepts of linear fits of α to t_{FM}^{-1} [Eq. (3)] that neglect TMS [Figs. 1(a) and 1(b)]. The estimates labeled "with TMS" are the results of full fits to Eq. (4) taking into account the TMS contribution [Figs. 2(c)–2(e)].

Series	FM	T_a (°C)	K_s (erg/cm^2)	α_{int} No TMS	α_{int} With TMS
1	NiFe		0.31±0.09	0.006	0.011
2	FeCoB		0.84±0.06	0.003	0.006
3	Co		0.90±0.07	0.001	0.011±0.001
4	Co	300	1.62±0.02	0.003±0.003	0.010±0.002
5	Co	350	2.52±0.02	−0.014±0.007	0.008±0.002
6	Co	450	3.27±0.02	−0.030±0.011	0.010±0.006

systems gives unphysical "giant" estimates for $G_{\mathrm{eff}}^{\uparrow\downarrow}$, and hence an incorrect quantification of spin-dependent transport phenomena across HM-FM interfaces and large errors in the determination of θ_{SH} and σ_{SH}.

For this Letter, we use six different series of sputter-deposited in-plane magnetized Pt-FM samples as examples (see Table I): (1) as-grown Pt/NiFe($Ni_{81}Fe_{19}$); (2) as-grown Pt/FeCoB($Fe_{60}Co_{20}B_{20}$); (3) as-grown Pt/Co; (4) Pt/Co, annealed at 300 °C; (5) Pt/Co, annealed at 350 °C; and (6) Pt/Co, annealed at 450 °C. The Pt thickness is 4 nm in all cases, while in each series t_{FM} was varied over a sufficient range to reveal the damping behavior. α was determined by spin-torque ferromagnetic resonance [36]. See the Supplemental Material [37] for more information on the samples and experimental methods.

In Figs. 1(a) and 1(b), we plot α as a function of t_{FM}^{-1} for the as-grown and annealed sample series, respectively. While α for the Pt/FeCoB samples varies quasilinearly with t_{FM}^{-1} over the full t_{FM} range, α for Pt/NiFe and Pt/Co sample series deviates markedly from the linear t_{FM}^{-1} scaling when t_{FM} is small. Focusing first on the large t_{FM} regime where α can be fit phenomenologically by a linear t_{FM}^{-1} dependence, as is typically done in the literature (i.e., $t_{\mathrm{FM}} >$ 3.5 nm for Pt/NiFe and Pt/Co series; $t_{\mathrm{FM}} > 2.2$ nm for Pt/FeCoB series), we determined $G_{\mathrm{eff},\alpha}^{\uparrow\downarrow}$ [Fig. 1(c)] and $g_{\mathrm{eff},\alpha}^{\uparrow\downarrow}$ for the different sample series from the fits of α to Eq. (3). $G_{\mathrm{eff},\alpha}^{\uparrow\downarrow}$ increases from $1.5\times10^{15}\ \Omega^{-1}\,\mathrm{m}^{-2}$ for the Pt/NiFe and Pt/FeCoB samples (series 1 and 2), to $1.8\times10^{15}\ \Omega^{-1}\,\mathrm{m}^{-2}$ for as-grown Pt/Co samples (series 3), and to $2.0\times10^{16}\ \Omega^{-1}\,\mathrm{m}^{-2}$ for Pt/Co annealed at 450 °C (sample series 6). Corresponding values of $g_{\mathrm{eff},\alpha}^{\uparrow\downarrow}$ are $4.0\times10^{19}\ \mathrm{m}^{-2}$ (series 1 and 2), $4.5\times10^{19}\ \mathrm{m}^{-2}$ (series 3), and $5.1\times10^{20}\ \mathrm{m}^{-2}$ (series 6). These $G_{\mathrm{eff},\alpha}^{\uparrow\downarrow}$ ($g_{\mathrm{eff},\alpha}^{\uparrow\downarrow}$) values for our as-grown Pt-FM samples are comparable to those reported from damping measurements on similar structures in the literature [9,11,13,16,24,42]. However, all of these values of $G_{\mathrm{eff},\alpha}^{\uparrow\downarrow}$ are markedly larger than the expected value $G_{\mathrm{eff}}^{\uparrow\downarrow} = 0.31\times10^{15}\ \Omega^{-1}\,\mathrm{m}^{-2}$, as calculated with Eq. (1) using the *ab initio* prediction $G_{\mathrm{Pt/Co}}^{\uparrow\downarrow} = 0.59\times10^{15}\ \Omega^{-1}\,\mathrm{m}^{-2}$ [18] and the experimentally determined $G_{\mathrm{Pt}} = 1.3\times10^{15}\ \Omega^{-1}\,\mathrm{m}^{-2}$ [20].

Moreover, while Eq. (1) requires that $G_{\mathrm{eff}}^{\uparrow\downarrow} \le G_{\mathrm{Pt}}/2$, all of the values of $G_{\mathrm{eff},\alpha}^{\uparrow\downarrow}$ we obtain using Eq. (3) are substantially larger than $G_{\mathrm{Pt}}/2$, with the ratio $G_{\mathrm{eff},\alpha}^{\uparrow\downarrow}/(G_{\mathrm{Pt}}/2)$ as large as 30 for Pt/Co series annealed at 450 °C. When $G_{\mathrm{eff}}^{\uparrow\downarrow} > G_{\mathrm{HM}}/2$, the value of $G_{\mathrm{HM\text{-}FM}}^{\uparrow\downarrow} = G_{\mathrm{eff}}^{\uparrow\downarrow}/(1-2G_{\mathrm{eff}}^{\uparrow\downarrow}/G_{\mathrm{HM}})$ will be negative, which is unphysical. Our group has also observed values of $G_{\mathrm{eff}}^{\uparrow\downarrow}$ much larger than $G_{\mathrm{HM}}/2$ from damping studies of Pt/CoFe [32] and PtMn/(FeCoB, Co) systems [28]. A giant $G_{\mathrm{eff}}^{\uparrow\downarrow}$ may be consistent with the bound ($G_{\mathrm{eff}}^{\uparrow\downarrow} < G_{\mathrm{HM}}/2$) in Eq. (1) only if λ_s is much shorter (e.g., <0.06 nm for Pt/Co annealed at 450 °C) than determined by independent measurements (~2 nm) [11]. However, this is also unphysical because it implies a value for $G_{\mathrm{HM\text{-}FM}}^{\uparrow\downarrow}$ that is much greater than the Sharvin conductance of Pt ($G_{\mathrm{Sh}} = 0.68\times10^{15}\ \Omega^{-1}\,\mathrm{m}^{-2}$) [43]. Note that the drift-diffusion model [4,17] and Eq. (1) require $G_{\mathrm{eff}}^{\uparrow\downarrow} < G_{\mathrm{HM\text{-}FM}}^{\uparrow\downarrow} \le G_{\mathrm{Sh}}$. Notably, the failure of the assumption of spin pumping dominating the FM thickness dependence of α and the deduced unphysical, giant $G_{\mathrm{eff},\alpha}^{\uparrow\downarrow}$ are not particular to Pt-FM systems, but it is generally observed for other HM-FM systems, including $Pd_{0.25}Pt_{0.75}$/(Co, FeCoB), $Au_{0.25}Pt_{0.75}$/(Co, FeCoB), Pd/Co, and W/FeCoB [37].

Variations of ξ_{DL}^{E} between the different Pt-FM series provide another illustration of the danger of misinterpreting these giant $G_{\mathrm{eff},\alpha}^{\uparrow\downarrow}$. Figure 1(d) plots ξ_{DL}^{E} from harmonic response measurements [19,20,44] on the representative samples of each series (i.e., Pt 4/NiFe 1.8 for series 1, Pt 4/FeCoB 2.8 for series 2, Pt 4/Co 3.2 for series 3–6) as a function of $G_{\mathrm{eff},\alpha}^{\uparrow\downarrow}$. For an ideal Pt-FM interface where T_{int} is set only by SBF, according to Eq. (2), a large $G_{\mathrm{eff}}^{\uparrow\downarrow}$ should favor a high ξ_{DL}^{E}. However, we find experimentally that ξ_{DL}^{E} decreases substantially and monotonically with increasing $G_{\mathrm{eff},\alpha}^{\uparrow\downarrow}$. Both the unphysically large $G_{\mathrm{eff},\alpha}^{\uparrow\downarrow}/(G_{\mathrm{Pt}}/2)$ ratios and the anticorrelation between ξ_{DL}^{E} and $G_{\mathrm{eff},\alpha}^{\uparrow\downarrow}$ provide unambiguous evidence that the values of $G_{\mathrm{eff},\alpha}^{\uparrow\downarrow}$ determined from the standard spin-pumping model, Eq. (3), are not accurate estimates of $G_{\mathrm{eff}}^{\uparrow\downarrow}$ defined by Eq. (1).

It has been established that SML due to the ISOC at the Pt-FM interfaces [12,31–35] provides an additional spin sink that can increase α and degrade T_{int} for the HM-FM interface. However, we find that the giant $G_{\mathrm{eff},\alpha}^{\uparrow\downarrow}$ values are not due primarily to SML. First, spin pumping into the SML interface should yield a t_{FM}^{-1} dependence for α and cannot explain the strong deviation from a t_{FM}^{-1} dependence

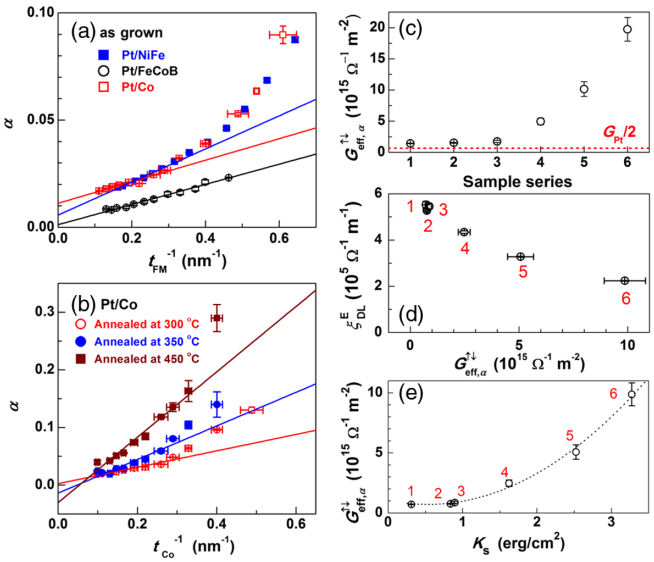

FIG. 1. Dependence of α on t_{FM}^{-1} for (a) the as-grown Pt/NiFe, Pt/FeCoB, and Pt/Co sample series and (b) the annealed Pt/Co sample series. The straight lines represent linear fits in the thick FM region [Eq. (3)]. (c) $g^{\uparrow\downarrow}_{eff,\alpha}$ and $G^{\uparrow\downarrow}_{eff,\alpha}$ for the different Pt-FM interfaces determined from the linear fits of α vs t_{FM}^{-1} [Eq. (3)]. The red dashed line represents $G_{Pt}/2 = 0.65 \times 10^{15}$ Ω^{-1} m^{-2}, an *upper* bound for the true $G^{\uparrow\downarrow}_{eff}$. (d) ξ^E_{DL} vs $G^{\uparrow\downarrow}_{eff,\alpha}$. (e) $G^{\uparrow\downarrow}_{eff,\alpha}$ vs K_s. The numbers 1–6 in (d) and (e) label the sample series.

that we find in the thin t_{FM} regime [Figs. 1(a) and 1(b)]. Second, if the enhancement in $G^{\uparrow\downarrow}_{eff,\alpha}$ by a factor of 20 from sample series 1–6 [Fig. 1(d)] were due to SML, ξ^E_{DL} should be reduced by a similarly large factor, rather than being reduced only by 25%. Finally, we find that $G^{\uparrow\downarrow}_{eff,\alpha}$ scales approximately as the *square* of the interfacial magnetic anisotropy energy density (K_s) at the Pt-FM interfaces [Fig. 1(e)] as determined by measuring the effective demagnetization field M_{eff} using ferromagnetic resonance and fitting to a t_{FM}^{-1} dependence [37]. In contrast, theory predicts that the contribution from SML should be linear in the ISOC strength [14], and therefore in K_s [33].

A third possible contribution to enhanced damping that has been seldom considered when analyzing interfacial spin transport is TMS [29] due to magnetic defects (roughness) at the interfaces (see Fig. S5 in the Supplemental Material [37]). As we next discuss, TMS dominates the enhancement of α in the Pt-FM heterostructures. A signature for the TMS contribution to the damping (α_{TMS}) is that, to the first approximation, it is a parabolic function of the interfacial perpendicular magnetic anisotropy field $2K_s/M_s t_{FM}$ [29,30]. If α_{TMS} is significant, the total damping is given approximately by $\alpha = \alpha_{int} + \alpha_{SP} + \alpha_{TMS}$ or

$$\alpha = \alpha_{int} + (G^{\uparrow\downarrow}_{eff} + G_{SML})\frac{g\mu_B h}{4\pi M_s e^2} t_{FM}^{-1} + \beta_{TMS} t_{FM}^{-2}, \quad (4)$$

where the second term is the combined contribution from spin pumping into the Pt layer and from SML at the interface, which for convenience we parametrize as an "effective SML conductance" G_{SML} [16,27], and β_{TMS} is a coefficient that depends on both $(K_s/M_s)^2$ and the density of magnetic defects at the FM surfaces [29,30]. (We provide further justification for the t_{FM}^{-2} dependence of the TMS term in the Supplemental Material [37]).

To properly fit the damping data to Eq. (4) and disentangle the different contributions, we must first estimate $G^{\uparrow\downarrow}_{eff}$ for the spin pumping into the Pt layer and G_{SML} for the spin pumping into the SML interface for the different Pt-FM series. We note that the expected value of $G^{\uparrow\downarrow}_{eff} = 0.31 \times 10^{15}$ Ω^{-1} m^{-2} for the Pt/Co interface [Eq. (1)] is in reasonable agreement with the experimental value of $G^{\uparrow\downarrow}_{eff,\alpha}$ obtained in Pt-FM samples [32,42], where the interfaces were engineered to reduce ISOC, and thereby minimize SML and TMS. For example, the damping measurements [Eq. (3)] have yielded $G^{\uparrow\downarrow}_{eff,\alpha} = 0.38 \times 10^{15}$ Ω^{-1} m^{-2} for unannealed CoFe/Pt bilayers [32] and $G^{\uparrow\downarrow}_{eff,\alpha} = 0.25 \times 10^{15}$ Ω^{-1} m^{-2} for Pt/FeCoB bilayers where ISOC (TMS and SML) was diminished by inserting a 0.5 nm Hf passivation spacer [37]. This indicates that $G^{\uparrow\downarrow}_{eff} = 0.31 \times 10^{15}$ Ω^{-1} m^{-2} is a reasonable approximation for all of the Pt-FM samples. To account for the SML contribution, we identify the reduction in ξ^E_{DL} with increasing ISOC [Figs. 1(e) and 2(a)] as being due to SML and assume that the fraction of spin current absorbed by SML at the interface is the same for the spin-pumping (FM → HM) and SOT (HM → FM) processes. Based on this approximation, we obtain

$$G_{SML} \approx G^{\uparrow\downarrow}_{eff}\frac{\xi^E_{DL}(\text{no SML}) - \xi^E_{DL}}{\xi^E_{DL}}. \quad (5)$$

Previous work [33] has established that ξ^E_{DL} deceases linearly with ISOC strength at the HM-FM interfaces ($K_s^{HM\text{-}FM}$) due to SML. In Fig. 2(a), we determine the baseline value of $\xi^E_{DL}(\text{no SML}) = (5.9 \pm 0.1) \times 10^5$ Ω^{-1} m^{-1} as determined from the linear $K_s^{Pt/Co}$ dependence of ξ^E_{DL} for Pt/Co bilayers. Using the measured ξ^E_{DL}, Eq. (5) yields the values of G_{SML} shown in Fig. 2(b). We find that G_{SML} is negligible relative to $G^{\uparrow\downarrow}_{eff}$ for the unannealed samples, but as a function of increasing annealing temperature, G_{SML} becomes comparable to and then larger than $G^{\uparrow\downarrow}_{eff}$.

With the values of $G^{\uparrow\downarrow}_{eff}$ and G_{SML} in Fig. 2(b), the damping data for all of the Pt-FM series can be fit well by Eq. (4) over the whole range of t_{FM} studied, using the two fitting parameters β_{TMS} and α_{int} [see Figs. 2(c)–2(e)]. As shown in Figs. 2(c) and 2(d), $\alpha_{TMS} = \beta_{TMS} t_{FM}^{-2}$ (red line) for both the Pt/NiFe and Pt/FeCoB sample series is larger than α_{SP} (blue line) in the whole range of t_{FM}. For the Pt/Co

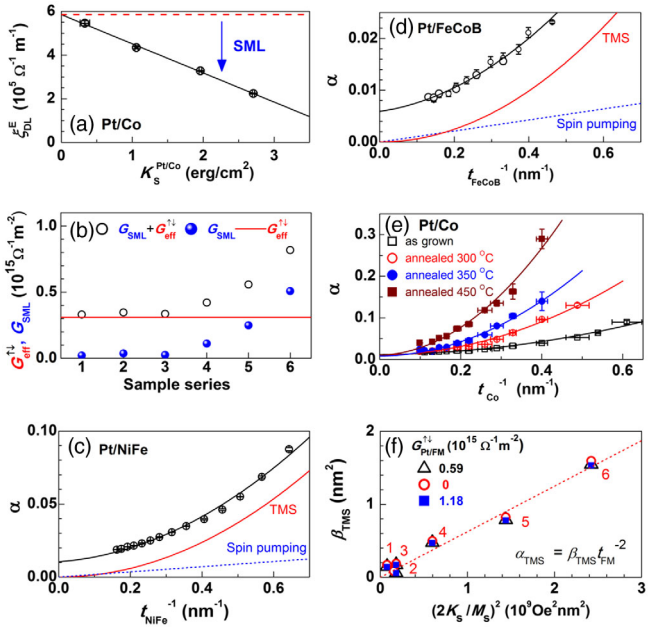

FIG. 2. (a) Reduction of ξ^E_{DL} for Pt 4/Co 3.2 bilayers with increasing $K_s^{\mathrm{Pt/Co}}$, indicating an extrapolated value of $\xi^E_{\mathrm{DL}} = 5.9 \times 10^5\ \Omega^{-1}\ \mathrm{m}^{-1}$ for zero SML (and zero ISOC) at the Pt/Co interface. (b) G_{SML}, $G^{\uparrow\downarrow}_{\mathrm{eff}}$, and the sum of the two. Damping for (c) Pt/NiFe, (d) Pt/FeCoB, and (e) Pt/Co plotted as a function of t_{FM}^{-1}. In (c) and (d), the black lines represent best fits of the data to Eq. (4) including the TMS contribution; the solid red and the dashed blue lines indicate, respectively, the TMS contribution and the total contribution of spin pumping into the Pt and the SML layer. In (e), the solid lines represent best fits of the data to Eq. (4). The intercepts in (c)–(e) indicate the intrinsic damping of the FM layer (the values in Table I labeled "with TMS"). (f) β_{TMS} vs $(2K_s/M_s)^2$ as determined by fits to Eq. (4) assuming different values of $G^{\uparrow\downarrow}_{\mathrm{Pt\text{-}FM}}$: $0, 0.59 \times 10^{15}$, and $1.18 \times 10^{15}\ \Omega^{-1}\ \mathrm{m}^{-2}$. The red numbers 1–6 in (f) label the sample series.

samples (series 3–6), the dominant parabolic scaling of α with t_{FM}^{-1} becomes increasingly stronger with increasing annealing temperature (and therefore increasing K_s) [Fig. 2(e)]. These observations demonstrate that TMS constitutes the largest thickness-dependent contribution to α for all of the Pt-FM systems we have examined, even for Pt/FeCoB ($K_s = 0.84 \pm 0.06\ \mathrm{erg/cm^2}$), where α appears to vary quasilinearly with t_{FM}^{-1} [Fig. 1(a)]. We also find that, for Pt/Co samples (series 3–6) with a similar structural roughness at the interfaces, the TMS coefficient β_{TMS} determined from the best fits in Figs. 2(c)–2(e) scales monotonically with $(2K_s/M_s)^2$ [Fig. 2(f)], in good agreement with the TMS mechanism [29,30]. β_{TMS} for Pt/FeCoB samples is ~3 times smaller than that of the as-grown Pt/Co and Pt/NiFe samples despite their similar values of $(2K_s/M_s)^2$, which indicates a smaller magnetic roughness at the amorphous FeCoB surfaces than at the polycrystalline NiFe and Co surfaces, where the last two show columnar growth on top of Pt (see Fig. S5 in the Supplemental Material [37]). Because $\alpha_{\mathrm{SP}} \ll \alpha_{\mathrm{TMS}}$ for most FM thicknesses (particularly in the small t_{FM} range), our conclusions are not sensitive to the details of the fitting procedure. As shown in Fig. 2(f), the fits of α to Eq. (4) give essentially the same β_{TMS} values for the different Pt-FM series whether we assume $G^{\uparrow\downarrow}_{\mathrm{Pt\text{-}FM}} = 0, 0.59 \times 10^{15}$ (theory [17]) or $1.18 \times 10^{15}\ \Omega^{-1}\ \mathrm{m}^{-2}$. Since α_{TMS} dominates α, the accuracy of the above conclusions are robust against any potential limitations of the drift-diffusion analysis [17,18].

For the HM–yttrium iron garnet (YIG) (e.g., HM = Pt, Ta, W, Cu) bilayers [45], we find both conditions of Eq. (1) (i.e., $G^{\uparrow\downarrow}_{\mathrm{eff}} < G_{\mathrm{HM}}/2$ and $G^{\uparrow\downarrow}_{\mathrm{eff}} < G^{\uparrow\downarrow}_{\mathrm{HM\text{-}FM}} \leq G_{\mathrm{Sh}}$) may be satisfied only when the real G_{HM} values are much smaller than used in the literature [45] (see the Supplemental Material [37]). This most likely suggests that the TMS is weak in those HM-YIG bilayers where the YIG layers are very thick (>20 nm [45]), but that the λ_s values of the HMs were considerably overestimated, and thus the θ_{SH} values were underestimated in those spin-pumping–ISHE experiments.

In a damping analysis for HM-FM bilayers where only spin pumping is considered, the t_{FM}-independent contribution, the intercept of the linear t_{FM}^{-1} fit of α using Eq. (3), is typically ascribed to the intrinsic α_{int} of the FM layer. However, the *apparent* α_{int} obtained from such linear t_{FM}^{-1} fits of α is often unphysically small or even negative; e.g., it is negative for Pt/Co and Pt/NiFe in Ref. [32]. As revealed by our numerical simulation [37], this is because α_{TMS} always contributes to a negative intercept in the fit of α to Eq. (3) in the thick FM region. As we summarize in Table I, for our samples, we observe similar fitting behaviors, and the linear t_{FM}^{-1} fits of total damping α in the thick FM region yield very small α_{int} for the as-grown Pt-FM sample sets [Fig. 1(a)] and negative α_{int} for annealed Pt/Co sample sets (Fig. S4 in the Supplemental Material [37]). Including the effects of TMS on α [Figs. 2(c)–2(e)] resolves this problem and yields reasonable α_{int} values (~0.011 for NiFe, ~0.006 for FeCoB, and ~0.010 for Co), which are in accord with the literature values for freestanding thin films of these materials [46,47]. We observe similar effects in many other HM-FM sample series [see the Supplemental Material [37] for more examples on $(\mathrm{Pd}_{0.25}\mathrm{Pt}_{0.75}, \mathrm{Au}_{0.25}\mathrm{Pt}_{0.75}, \mathrm{Pd})$/Co and $(\mathrm{Pd}_{0.25}\mathrm{Pt}_{0.75}, \mathrm{Au}_{0.25}\mathrm{Pt}_{0.75}, \mathrm{W})$/FeCoB sample series]. This finding therefore indicates that TMS must be taken into account when estimating α_{int} of a FM from its thickness dependence.

The understanding that our analysis provides about the relative strength of TMS, SML, and spin pumping, and how these processes depend on the ISOC strength, has wide-ranging implications for correctly understanding spin current transport at HM-FM interfaces. As aforementioned, ξ^E_{DL} can vary inversely with $G^{\uparrow\downarrow}_{\mathrm{eff},\alpha}$ even though, according to Eq. (2), it should increase with increases in true $G^{\uparrow\downarrow}_{\mathrm{eff}}$. Similarly, voltage signals in spin-pumping–ISHE

measurements in Pt-FM samples can vary inversely with $G^{\uparrow\downarrow}_{\mathrm{eff},\alpha}$ [48] even though they are expected to scale $\propto G^{\uparrow\downarrow}_{\mathrm{eff}}\theta_{\mathrm{SH}}$. These puzzles are resolved if the dominant contribution to $G^{\uparrow\downarrow}_{\mathrm{eff},\alpha}$ is TMS, which does not affect spin transport across the interface. In addition, previous observations of an increase of $G^{\uparrow\downarrow}_{\mathrm{eff},\alpha}$ with the FM roughness [49], and scaling of $G^{\uparrow\downarrow}_{\mathrm{eff},\alpha}$ at HM-CoFeB interfaces with the interfacial Dzyaloshinskii-Moriya interaction constant (a factor that is proportional to the ISOC strength) [50] can be natural consequences of TMS. We note that α has been reported to be much larger in some HM-FM structures (e.g., Pt/CoFe [19] or PtMn/FeCoB [28]) than in the corresponding reversed order structures (i.e., FM-HM) despite their similar SOT strengths. This is consistent with a stronger α_{TMS} due to a larger magnetic roughness when the FM is grown on top of the HM. The dominant role of TMS in determining α in the thin HM-FM systems also explains observations that the reduction of ISOC at the HM-FM interface by a Hf atomic layer insertion can dramatically reduce α in Pt/Co, Pt/FeCoB, and W/FeCoB systems without materially decreasing T_{int} for the diffusion of spins from the HM layer into the FM layer [33,37,51].

Our results also indicate an critical need to reevaluate all measurements of θ_{SH} and σ_{SH} that utilize $G^{\uparrow\downarrow}_{\mathrm{eff},\alpha}$ from damping measurements to estimate the true $G^{\uparrow\downarrow}_{\mathrm{eff}}$. Given that the measured signal strengths scale as $\propto G^{\uparrow\downarrow}_{\mathrm{eff}}\theta_{\mathrm{SH}}$ in spin-pumping–ISHE and SSE-ISHE measurements and $\propto G^{\uparrow\downarrow}_{\mathrm{eff}}\theta^2_{\mathrm{SH}}$ in SMR measurements, the common use of $G^{\uparrow\downarrow}_{\mathrm{eff},\alpha}$ as a proxy for $G^{\uparrow\downarrow}_{\mathrm{eff}}$ means that most values of θ_{SH} in the literature determined by these techniques significantly underestimate the correct values. SOT measurements are often quoted as providing only a lower bound on θ_{SH} or σ_{SH}, assuming only that $T_{\mathrm{int}} \leq 1$. While these lower bounds remain accurate, the improved understanding of $G^{\uparrow\downarrow}_{\mathrm{eff}}$ from our analysis allows a more-confident quantification of T_{int}, so as to provide accurate measurements of θ_{SH} or σ_{SH} using SOT experiments. By the analysis associated with Fig. 2, the values of T_{int} for our Pt 4–FM sample series vary with the strength of ISOC such that $T_{\mathrm{int}} \approx 0.38$ for samples series 1–3, 0.30 for series 4, 0.23 for series 5, and 0.16 for series 6. In all cases, our data are consistent with $\sigma_{\mathrm{SH}} \approx 1.5 \times 10^6 (\hbar/2e)\ \Omega^{-1}\,\mathrm{m}^{-1}$ or $\theta_{\mathrm{SH}} = 0.64$ within Pt given an average resistivity of $\rho_{xx} = 40\ \mu\Omega\,\mathrm{cm}$. These values are consistent with previous estimates in Ref. [33].

In conclusion, two-magnon scattering rather than spin pumping is the dominant contribution to the FM-thickness dependence of α for in-plane-magnetized HM-FM systems in the nanometer thickness and gigahertz frequency regions important for spintronics. SML at the interface can also play an important role in affecting both α and T_{int} when ISOC is strong. Neglecting the influence of TMS and SML, particularly the former, can lead to unphysical giant estimates for $G^{\uparrow\downarrow}_{\mathrm{eff}}$. A correct calculation of θ_{SH} and σ_{SH} therefore requires careful determination of the strength of both TMS and SML. Our findings also indicate that ISOC and magnetic roughness should be minimized in technological applications that benefit from low α.

Note that our analysis has employed the simplifying assumption that $G^{\uparrow\downarrow}_{\mathrm{eff}}$, and hence the degree of SBF, is approximately independent of the strength of SML, which is supported by the observed linear relationship between ξ^E_{DL} and $K_s^{\mathrm{Pt/Co}}$. A theoretical modeling of the possible interplay of $G^{\uparrow\downarrow}_{\mathrm{eff}}$ and SML is worthy of future efforts but is beyond the scope of this Letter.

This work was supported in part by the Office of Naval Research (Grant No. N00014-15-1-2449) and by the NSF MRSEC program (Grant No. DMR-1719875) through the Cornell Center for Materials Research. This work was performed in part at the Cornell NanoScale Facility, an NNCI member supported by NSF Grant No. ECCS-1542081.

*lz442@cornell.edu

[1] L. Liu, C.-F. Pai, Y. Li, H. W. Tseng, D. C. Ralph, and R. A. Buhrman, Spin-torque switching with the giant spin Hall effect of tantalum, Science **336**, 555 (2012).

[2] V. E. Demidov, S. Urazhdin, H. Ulrichs, V. Tiberkevich, A. Slavin, D. Baither, G. Schmitz, and S. O. Demokritov, Magnetic nano-oscillator driven by pure spin current, Nat. Mater. **11**, 1028 (2012).

[3] C. O. Avci, K. Garello, A. Ghosh, M. Gabureac, S. F. Alvarado, and P. Gambardella, Unidirectional spin Hall magnetoresistance in ferromagnet/normal metal bilayers, Nat. Phys. **11**, 570 (2015).

[4] Y.-T. Chen, S. Takahashi, H. Nakayama, M. Althammer, S. T. B. Goennenwein, E. Saitoh, and G. E. W. Bauer, Theory of spin Hall magnetoresistance, Phys. Rev. B **87**, 224401 (2013).

[5] K. Uchida, S. Takahashi, K. Harii, J. Ieda, W. Koshibae, K. Ando, S. Maekawa, and E. Saitoh, Observation of the spin Seebeck effect, Nature (London) **455**, 778 (2008).

[6] D. Meier, D. Reinhardt, M. van Straaten, C. Klewe, M. Althammer, M. Schreier, S. T. B. Goennenwein, A. Gupta, M. Schmid, C. H. Back, J.-M. Schmalhorst, T. Kuschel, and G. Reiss, Longitudinal spin Seebeck effect contribution in transverse spin Seebeck effect experiments in Pt/YIG and Pt/NFO, Nat. Commun. **6**, 8211 (2015).

[7] W. Lin, K. Chen, S. Zhang, and C. L. Chien, Enhancement of Thermally Injected Spin Current through an Antiferromagnetic Insulator, Phys. Rev. Lett. **116**, 186601 (2016).

[8] J. C. Rojas Sánchez, L. Vila, G. Desfonds, S. Gambarelli, J. P. Attané, J. M. De Teresa, C. Magén, and A. Fert, Spin-to-charge conversion using Rashba coupling at the interface between non-magnetic materials, Nat. Commun. **4**, 2944 (2013).

[9] X. Tao, Q. Liu, B. Miao, R. Yu, Z. Feng, L. Sun, B. You, J. Du, K. Chen, S. Zhang, L. Zhang, Z. Yuan, D. Wu, and H. Ding, Self-consistent determination of spin Hall angle and

spin diffusion length in Pt and Pd: The role of the interface spin loss, Sci. Adv. **4**, eaat1670 (2018).

[10] B. Heinrich, C. Burrowes, E. Montoya, B. Kardasz, E. Girt, Y.-Y. Song, Yiyan Sun, and M. Wu, Spin Pumping at the Magnetic Insulator (YIG)/Normal Metal (Au) Interfaces, Phys. Rev. Lett. **107**, 066604 (2011).

[11] M. Obstbaum, M. Decker, A. K. Greitner, M. Haertinger, T. N. G. Meier, M. Kronseder, K. Chadova, S. Wimmer, D. Ködderitzsch, H. Ebert, and C. H. Back, Tuning Spin Hall Angles by Alloying, Phys. Rev. Lett. **117**, 167204 (2016).

[12] K. Chen and S. Zhang, Spin Pumping in the Presence of Spin-Orbit Coupling, Phys. Rev. Lett. **114**, 126602 (2015).

[13] F. D. Czeschka, L. Dreher, M. S. Brandt, M. Weiler, M. Althammer, I.-M. Imort, G. Reiss, A. Thomas, W. Schoch, W. Limmer, H. Huebl, R. Gross, and S. T. B. Goennenwein, Scaling Behavior of the Spin Pumping Effect in Ferromagnet-Platinum Bilayers, Phys. Rev. Lett. **107**, 046601 (2011).

[14] O. Mosendz, J. E. Pearson, F. Y. Fradin, G. E. W. Bauer, S. D. Bader, and A. Hoffmann, Quantifying Spin Hall Angles from Spin Pumping: Experiments and Theory, Phys. Rev. Lett. **104**, 046601 (2010).

[15] F. D. Czeschka, L. Dreher, M. S. Brandt, M. Weiler, M. Althammer, I.-M. Imort, G. Reiss, A. Thomas, W. Schoch, W. Limmer, H. Huebl, R. Gross, and S. T. B. Goennenwein, Scaling Behavior of the Spin Pumping Effect in Ferromagnet-Platinum Bilayers, Phys. Rev. Lett. **107**, 046601 (2011).

[16] J.-C. Rojas-Sánchez, N. Reyren, P. Laczkowski, W. Savero, J.-P. Attané, C. Deranlot, M. Jamet, J.-M. George, L. Vila, and H. Jaffrès, Spin Pumping and Inverse Spin Hall Effect in Platinum: The Essential Role of Spin-Memory Loss at Metallic Interfaces, Phys. Rev. Lett. **112**, 106602 (2014).

[17] P. M. Haney, H. W. Lee, K. J. Lee, A. Manchon, and M. D. Stiles, Current induced torques, and interfacial spin-orbit coupling: Semiclassical modeling, Phys. Rev. B **87**, 174411 (2013).

[18] V. P. Amin and M. D. Stiles, Spin transport at interfaces with spin-orbit coupling: Phenomenology, Phys. Rev. B **94**, 104420 (2016).

[19] C.-F. Pai, Y. Ou, L. H. Vilela-Leao, D. C. Ralph, and R. A. Buhrman, Dependence of the efficiency of spin Hall torque on the transparency of Pt/ferromagnetic layer interfaces, Phys. Rev. B **92**, 064426 (2015).

[20] M.-H. Nguyen, D. C. Ralph, and R. A. Buhrman, Spin Torque Study of the Spin Hall Conductivity and Spin Diffusion Length in Platinum Thin Films with Varying Resistivity, Phys. Rev. Lett. **116**, 126601 (2016).

[21] L. Zhu, D. C. Ralph, and R. A. Buhrman, Highly Efficient Spin Current Generation by the Spin Hall Effect in $Au_{1-x}Pt_x$, Phys. Rev. Applied **10**, 031001 (2018).

[22] L. J. Zhu, K. Sobotkiewich, X. Ma, X. Li, D. C. Ralph, and R. A. Buhrman, Strong damping-like spin-orbit torque and tunable Dzyaloshinskii–Moriya interaction generated by low-resistivity $Pd_{1-X}Pt_X$ alloys, Adv. Funct. Mater. **29**, 1805822 (2019).

[23] L. J. Zhu, D. C. Ralph, and R. A. Buhrman, Irrelevance of magnetic proximity effect to the spin-orbit torques in heavy metal/ferromagnet bilayers, Phys. Rev. B **98**, 134406 (2018).

[24] W. Zhang, W. Han, X. Jiang, S.-H. Yang, and S. S. P. Parkin, Role of transparency of platinum-ferromagnet interfaces in determining the intrinsic magnitude of the spin Hall effect, Nat. Phys. **11**, 496 (2015).

[25] L. Soumah, N. Beaulieu, L. Qassym, C. Carrétéro, E. Jacquet, R. Lebourgeois, J. B. Youssef, P. Bortolotti, V. Cros, and A. Anane, Ultra-low damping insulating magnetic thin films get perpendicular, Nat. Commun. **9**, 3355 (2018).

[26] M. C. Wheeler, F. Al MaMari, M. Rogers, F. J. Gonçalves, T. Moorsom, A. Brataas, R. Stamps, M. Ali, G. Burnell, B. J. Hickey, and O. Cespedes, Optical conversion of pure spin currents in hybrid molecular devices, Nat. Commun. **8**, 926 (2017).

[27] A. J. Berger, E. R. J. Edwards, H. T. Nembach, O. Karis, M. Weiler, and T. J. Silva, Determination of the spin Hall effect and the spin diffusion length of Pt from self-consistent fitting of damping enhancement and inverse spin-orbit torque measurements, Phys. Rev. B **98**, 024402 (2018).

[28] Y. Ou, S. Shi, D. C. Ralph, and R. A. Buhrman, Strong spin Hall effect in the antiferromagnet PtMn, Phys. Rev. B **93**, 220405(R) (2016).

[29] R. Arias and D. L. Mills, Extrinsic contributions to the ferromagnetic resonance response of ultrathin films, Phys. Rev. B **60**, 7395 (1999).

[30] A. Azevedo, A. B. Oliveira, F. M. de Aguiar, and S. M. Rezende, Extrinsic contributions to spin-wave damping and renormalization in thin $Ni_{50}Fe_{50}$ films, Phys. Rev. B **62**, 5331 (2000).

[31] Y. Liu, Z. Yuan, R. J. H. Wesselink, A. A. Starikov, and P. J. Kelly, Interface Enhancement of Gilbert Damping from First Principles, Phys. Rev. Lett. **113**, 207202 (2014).

[32] K. Dolui and B. K. Nikolic, Spin-memory loss due to spin-orbit coupling at ferromagnet/heavy-metal interfaces: *Ab initio* spin-density matrix approach, Phys. Rev. B **96**, 220403 (R) (2017).

[33] L. Zhu, D. C. Ralph, and R. A. Buhrman, Spin-Orbit Torques in Heavy-Metal-Ferromagnet Bilayers with Varying Strengths of Interfacial Spin-Orbit Coupling, Phys. Rev. Lett. **122**, 077201 (2019).

[34] K. D. Belashchenko, Alexey A. Kovalev, and M. van Schilfgaarde, Theory of Spin Loss at Metallic Interfaces, Phys. Rev. Lett. **117**, 207204 (2016).

[35] L. Zhu, D. C. Ralph, and R. A. Buhrman, Enhancement of spin transparency by interfacial alloying, Phys. Rev. B **99**, 180404(R) (2019).

[36] L. Liu, T. Moriyama, D. C. Ralph, and R. A. Buhrman, Spin-torque Ferromagnetic Resonance Induced by the Spin Hall Effect, Phys. Rev. Lett. **106**, 036601 (2011).

[37] See Supplemental Material at http://link.aps.org/supplemental/10.1103/PhysRevLett.123.057203, which includes Refs. [38–41], for more information on sample preparation and measurement methods, determination of interfacial anisotropy energy density, numerical simulation of the magnetic damping due to two-magnon scattering, more examples on the FM thickness dependence of damping of HM-FM bilayers, and magnetic roughness.

[38] N. Nakajima, T. Koide, T. Shidara, H. Miyauchi, H. Fukutani, A. Fujimori, K. Iio, T. Katayama, M. Nývlt, and Y. Suzuki, Perpendicular Magnetic Anisotropy Caused by Interfacial Hybridization via Enhanced Orbital Moment in Co/Pt Multilayers: Magnetic Circular X-Ray Dichroism Study, Phys. Rev. Lett. **81**, 5229 (1998).

[39] M. Suzuki, H. Muraoka, Y. Inaba, H. Miyagawa, N. Kawamura, T. Shimatsu, H. Maruyama, N. Ishimatsu, Y. Isohama, and Y. Sonobe, Depth profile of spin and orbital magnetic moments in a subnanometer Pt film on Co, Phys. Rev. B **72**, 054430 (2005).

[40] C. Kittel, On the theory of ferromagnetic resonance absorption, Phys. Rev. **73**, 155 (1948).

[41] J. Kim, P. Sheng, S. Takahashi, S. Mitani, and M. Hayashi, Spin Hall Magnetoresistance in Metallic Bilayers, Phys. Rev. Lett. **116**, 097201 (2016).

[42] M.-H. Nguyen, C.-F. Pai, K. X. Nguyen, D. A. Muller, D. C. Ralph, and R. A. Buhrman, Enhancement of the anti-damping spin torque efficacy of platinum by interface modification, Appl. Phys. Lett. **106**, 222402 (2015).

[43] M. Zwierzycki, Y. Tserkovnyak, P. Kelly, A. Brataas, and G. E. W. Bauer, First-principles study of magnetization relaxation enhancement and spin transfer in thin magnetic films, Phys. Rev. B **71**, 064420 (2005).

[44] C. O. Avci, K. Garello, M. Gabureac, A. Ghosh, A. Fuhrer, S. F. Alvarado, and P. Gambardella, Interplay of spin-orbit torque and thermoelectric effects in ferromagnet/normal-metal bilayers, Phys. Rev. B **90**, 224427 (2014).

[45] H. L. Wang, C. H. Du, Y. Pu, R. Adur, P. C. Hammel, and F. Y. Yang, Scaling of Spin Hall Angle in 3*d*, 4*d*, and 5*d* Metals from $Y_3Fe_5O_{12}$/ Metal Spin Pumping, Phys. Rev. Lett. **112**, 197201 (2014).

[46] S. Ingvarsson, L. Ritchie, X. Y. Liu, Gang Xiao, J. C. Slonczewski, P. L. Trouilloud, and R. H. Koch, Role of electron scattering in the magnetization relaxation of thin $Ni_{81}Fe_{19}$ films, Phys. Rev. B **66**, 214416 (2002).

[47] M. Oogane, T. Wakitani, S. Yakata, R. Yilgin, Y. Ando, A. Sakuma, and T. Miyazaki, Magnetic damping in ferromagnetic thin films, Jpn. J. Appl. Phys. **45**, 3889 (2006).

[48] A. Conca, B. Heinz, M. R. Schweizer, S. Keller, E. Th. Papaioannou, and B. Hillebrands, Lack of correlation between the spin-mixing conductance and the inverse spin Hall effect generated voltages in CoFeB/Pt and CoFeB/Ta bilayers, Phys. Rev. B **95**, 174426 (2017).

[49] T. K. H. Pham, M. Ribeiro, J. H. Park, N. J. Lee, K. Hoon Kang, E. Park, V. Q. Nguyen, A. Michel, C. S. Yoon, S. Cho, and T. H. Kim, Interface morphology effect on the spin mixing conductance of Pt/Fe_3O_4 bilayers, Sci. Rep. **8**, 13907 (2018).

[50] X. Ma, G. Yu, C. Tang, X. Li, C. He, J. Shi, K. L. Wang, and X. Li, Interfacial Dzyaloshinskii-Moriya Interaction: Effect of 5*d* Band Filling and Correlation with Spin Mixing Conductance, Phys. Rev. Lett. **120**, 157204 (2018).

[51] C.-F. Pai, M.-H. Nguyen, C. Belvin, L. H. Vilela-Leão, D. C. Ralph, and R. A. Buhrman, Enhancement of perpendicular magnetic anisotropy and transmission of spin-Hall-effect- induced spin currents by a Hf spacer layer in W/Hf/CoFeB/MgO layer structures, Appl. Phys. Lett. **104**, 082407 (2014).